

# Nonlinear Network Analysis and Measurement

Peter S. Blockley<sup>(1)</sup>, Jonathan B. Scott<sup>(2)</sup>, Daniel Gunyan<sup>(3)</sup> and Anthony E. Parker<sup>(4)</sup>,

<sup>(1)</sup> *Department of Electronics, Macquarie University, Sydney AUSTRALIA 2109,  
mailto: peterblockley@ieee.org*

<sup>(2)</sup> *Microwave Technology Center, Agilent Technologies. 1400 Fountaingrove Parkway, Santa Rosa, USA, 95404  
mailto: jonathanscott@ieee.org*

<sup>(3)</sup> *As (2) above, but mailto: daniel.gunyan@ieee.org*

<sup>(4)</sup> *As (1) above, but mailto: tonyp@ics.mq.edu.au*

## ABSTRACT

A measurement system that enables next generation broadband communications systems is described. The measurements are fully calibrated and are traceable to the national standards laboratories. The system has immediate applications in the deployment of wide-bandwidth, power efficient, low-cost telecommunications infrastructure. It also has potential applications in automotive radar for collision detection, delivery of broadband Internet and high definition TV to homes and other novel applications with large bandwidth requirements.

## INTRODUCTION

A measurement setup is described that performs wide-bandwidth, calibrated measurements of signals and systems. It measures complex modulated signals at two ports that are calibrated to an arbitrary reference plane. A new hardware platform, which provides superior performance over the existing methods has been developed. This includes increased sensitivity, accuracy, speed and improved bandwidth.

The project has included the development of new standards that have been fully characterized by the National Institute of Standards and Technology, the national standards laboratory in the United States. Thus, the response is fully traceable to this national standards laboratory.

The system not only tests devices but provides additional information for better modeling and compensation of nonlinearity. This opens up opportunities for exciting applications, such as compensation of nonlinearity in power amplifiers, for example. Nonlinearity in microwave power amplifiers results in a trade-off between spectrum usage and power consumption. This measurement system can be used to reduce power consumption in base stations, which results in a reduction in the physical size and cost of telecommunications installations.

The system provides wide-bandwidth (300 kHz - 20 GHz), high sensitivity (85 dB spurious-free dynamic range) and high accuracy due to the calibration, which we implemented. The bandwidth of the measurement system is similar to that of an oscilloscope, and the sensitivity is similar to that of a spectrum analyser or vector signal analyser. Unlike an oscilloscope, spectrum analyser or vector signal analyser, the new system is fully calibrated and traceable to the national standards laboratory.

The system can be used for making accurate multi-tone and complex modulation nonlinear measurements of system components. This enables simplified measurements with real-world excitations such as W-CDMA, multi-carrier signals for mobile phone base stations and Ultra-Wide-Band for short range communications.

The system's receivers are mixer-based, which provides both increased measurement speed and measurement sensitivity (dynamic range) compared to sampler based technologies. This combines the benefits of the high dynamic range available from the mixer-based hardware with a configuration which enables it to measure wide-bandwidth signals.

## MEASUREMENT SETUP

The measurement setup [1] is based on the Agilent N5230A 4-port, 20 GHz linear vector network analyzer that has been modified for 2-port, nonlinear operation. The block diagram for the system is shown in Fig. 1. The hardware consists of two receivers and two directional couplers for each port, plus an additional reference receiver. The directional couplers measure the traveling waves at each port, which are used during calibration and can be transformed to calculate the voltage and current spectrum.

The system not only returns the magnitude spectrum, but also the phase spectrum of the signal being measured. The phase information can be useful for analysing distortion or wide-bandwidth Error Vector Magnitude (EVM). With wide-bandwidth magnitude and phase information, the measurement result can also be transformed to the time-domain, such that the crest factor can be calculated or signal clipping observed.

The measurement system operates in the frequency domain in a similar fashion to a spectrum analyser. A local oscillator is swept across a frequency range and the tones of interest are mixed to an Intermediate Frequency (IF) where they are sampled. In a traditional spectrum analyser, the local oscillator synthesiser is not phase-coherent and the phase is unknown. Therefore the phase information is only useful in the narrow bandwidth of the IF filter.

The measurement system has the advantage of recovering the phase information of the local oscillator and hence the measurement. The phase of the local oscillator is recovered by measuring a signal with known relative phase. In practice the known signal is a repetitive impulse in the time domain, which contains many tones in the frequency domain. The impulse is highly repeatable, with the intention of being traceable to a national standards laboratory.

The raw phase returned by the hardware has a component due to the signal being measured and the local oscillator. If one measures the signal and reference simultaneously and then takes the difference between the phases, the corrected phase ( $\phi_C$ ) is given by:

$$\phi_C = (\phi_S + \phi_{lo}) - (\phi_R + \phi_{lo}) \quad (1)$$

$$\phi_C = \phi_S - \phi_R \quad (2)$$

where  $\phi_S$  is the phase of the sampled signal,  $\phi_R$  the measured phase of the reference and  $\phi_{lo}$  the phase of the local oscillator. The new phase  $\phi_C$  is no longer dependent on the phase of the local oscillator. Knowledge of the relative phase of the reference can then be used to recover the actual phase of the signal or the system can be calibrated against a second, external phase reference (as is done in practice). This operation can be performed using complex arithmetic as:

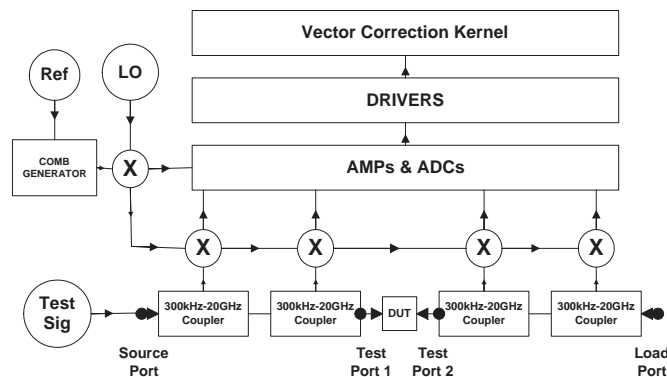


Fig. 1. Block diagram of the system. The hardware consists of two receivers and two directional couplers for each port, plus an additional reference receiver. The directional couplers measure the traveling waves at each port, which are used during calibration and allows the system to return not only the power spectrum at each port, but also the voltage and current spectrum.

$$X_C + jY_C = \frac{X_S + jY_S}{X_R + jY_R} |X_R + jY_R| \quad (3)$$

where  $X_S$  and  $Y_S$  are the real and imaginary parts of the sampled signal.  $X_R$  and  $Y_R$  are the real and imaginary parts of reference channel respectively.  $X_C$  and  $Y_C$  are the real and imaginary parts of the corrected result.

Modern spectrum analysers allow a scalar calibration performed against a power meter standard. This scalar calibration is unable to fully take into account mismatch loss at the test port or on-wafer transitions. The software for the new measurement system performs a full vector calibration, which is able to account for these losses.

## CALIBRATION AND CORRECTION

Although not a strict requirement, the system can be calibrated, such that the measurements are fully traceable to national standards laboratories. The calibration can be done at a connectorized plane, as demonstrated in [1] or at the wafer plane for characterizing on-wafer devices. The calibrations implemented use the model shown in Fig. 3. This is a standard 8-term model [2], which accounts for losses, phase shifts and mismatch at the ports, but assumes there is no signal leakage between the ports.

On-wafer calibration of a conventional linear vector network analyser, is a ratioed calibration. Once calibrated, the corrected measurements of reflection and transmission coefficients (ratio of incident, reflected and transmission waves) are returned, which can be translated to impedance or admittance matrices (ratio of voltage and current). A conventional linear vector network analyser returns only raw (uncorrected) data for incident, reflected and transmission waves (voltage and current).

The measurement system has an additional calibration step that enables it to return corrected incident, reflected and transmitted waves, which can then be transformed to voltage and current. This additional step is outlined in [3], although intended for a different hardware configuration. The calibration procedure uses a power meter for calibration of absolute magnitude and a phase reference for calibration of the phase. Both the power meter and phase reference are traceable to the national standards laboratory at a connectorized plane (a plug or socket such as Type N or SMA connector rather than on-chip).

The procedure for two-port on-wafer calibration is performed in two parts, a 1-port absolute calibration (resulting in the coefficients:  $A_{00}, A_{01}, A_{10}, A_{11}$ ) similar to that in [3] performed at a connectorized plane and a two-port ratioed calibration (see [2] for an overview of two-port calibrations) performed at the wafer plane (resulting in the coefficients:  $e_{00}, e_{11}, e_{22}, e_{33}, e_{01}e_{10}, e_{01}e_{10}$  and  $e_{01}e_{23}$ ).

Once the two calibrations have been performed, the absolute 1-port calibration is applied to the ratioed two-port calibration, to produce a two-port absolute calibration. This procedure is required to calculate the remaining coefficients ( $e_{01}, e_{10}, e_{23}, e_{32}$ ) of the two-port error model. This is achieved by noting that the X error adapter of the two-port calibration shown in Fig. 3 is composed of two error adapters A and B. Error adapter A represents the 1-port absolute

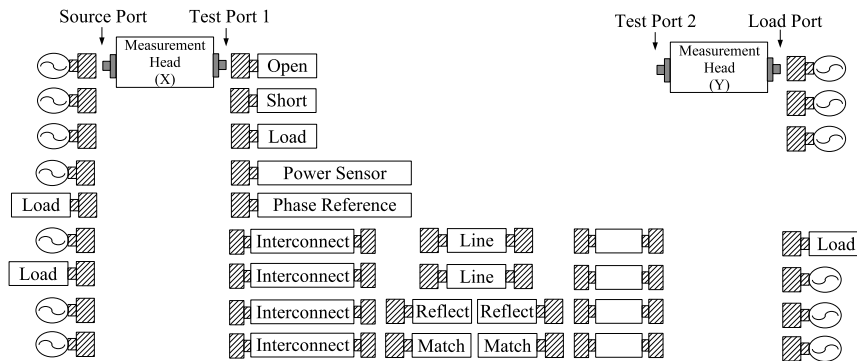


Fig. 2. Example of connections required for on-wafer Line-Reflect-Match (LRM) calibration. Two calibrations are performed, a one-port absolute calibration at a connectorized plane and a two-port ratioed calibration at the wafer plane.

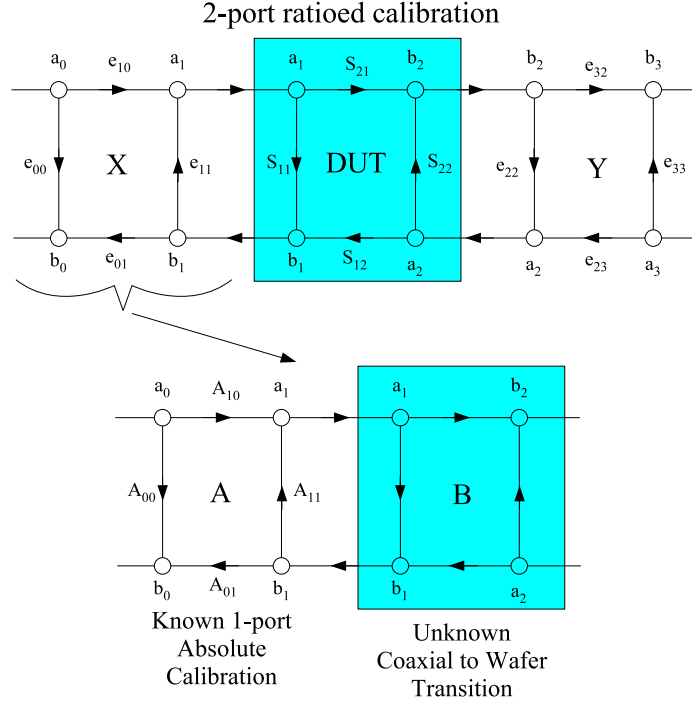


Fig. 3. An on-wafer calibration consists of two parts, a 1-port absolute calibration performed at a connectorized plane and a two-port radioed calibration performed at the wafer plane. The error matrix  $X$  of the two-port calibration is composed of the error matrix  $A$  of the absolute calibration and an error matrix  $B$  of the coaxial to wafer transition.

calibration, while error adapter  $B$  represents the coaxial to wafer transition. From the flow graph the following equality is derived:

$$\frac{1}{e_{10}} \begin{bmatrix} -\Delta_X & e_{00} \\ -e_{11} & 1 \end{bmatrix} = \frac{1}{A_{10}} \begin{bmatrix} -\Delta_A & A_{00} \\ -A_{11} & 1 \end{bmatrix} \begin{bmatrix} B_{11} & B_{12} \\ B_{21} & B_{22} \end{bmatrix} \quad (4)$$

where  $\Delta_A = A_{00}A_{11} - A_{01}A_{10}$  and  $\Delta_X = e_{00}e_{11} - e_{01}e_{10}$ . Solving for  $B$  gives:

$$\begin{bmatrix} B_{11} & B_{12} \\ B_{21} & B_{22} \end{bmatrix} = \frac{\begin{bmatrix} A_{00}e_{11} - \Delta_X & e_{00} - A_{00} \\ \Delta_A e_{11} - \Delta_X A_{11} & e_{00}A_{11} - \Delta_A \end{bmatrix}}{A_{01}e_{10}} \quad (5)$$

Given that the coaxial to wafer transition is reciprocal (the interconnect transfers power equally in either direction) then the  $B$  error adapter has the property:

$$B_{00}B_{11} - B_{01}B_{10} = 1 \quad (6)$$

substituting (5) into (6):

$$1 = \frac{(A_{00}e_{11} - \Delta_X)(e_{00}A_{11} - \Delta_A) - (e_{00} - A_{00})(\Delta_A e_{11} - \Delta_X A_{11})}{A_{01}^2 e_{10}^2} \quad (7)$$

$$e_{10} = \pm \frac{\sqrt{(A_{00}e_{11} - \Delta_X)(e_{00}A_{11} - \Delta_A) - (e_{00} - A_{00})(\Delta_A e_{11} - \Delta_X A_{11})}}{A_{01}} \quad (8)$$

With the presented information, there are two possible solutions for the error coefficient  $e_{10}$ . The correct solution is selected by knowledge of the approximate electrical length of the interconnect. An ideal lossless interconnect can be modeled with the following S-parameter matrix:

$$\begin{bmatrix} B_{00} & B_{01} \\ B_{10} & B_{11} \end{bmatrix} = \begin{bmatrix} 0 & e^{-j\omega\beta l} \\ e^{-j\omega\beta l} & 0 \end{bmatrix} \quad (9)$$

where  $\beta$  is the phase constant and  $l$  the electrical length of the interconnect. The measured transmission coefficient of a reciprocal interconnect is given by:

$$B_{01} = B_{10} = \frac{A_{01}e_{10}}{e_{00}A_{11} - \Delta_A} \quad (10)$$

Thus, the following inequality must be satisfied for the solution to be within  $\pm 90^\circ$  of the approximate electrical length:

$$\Re\left(\frac{e^{-j\omega\beta l}}{B_{01}}\right) > 0 \quad (11)$$

In this way an absolute calibration can be applied to any ratioed calibration. An example of the connections required for a two-port on-wafer Line-Reflect-Match (LRM) calibration is shown in Fig. 2. A similar procedure was first proposed in [4].

## DEFINING PHASE

Often nonlinear systems are characterized by only their magnitude spectrum. For instance verifying spectral mask compliance or determining the 3rd order intercept point of an amplifier only requires magnitude information. For advanced applications, such as device modeling and linearization, the phase spectrum provides important information and can be readily obtained over wide-bandwidths with the new measurement system.

The magnitude spectrum of a periodic signal is time-invariant, which means the spectrum is independent of time-shift as can be seen from the time-shifted Fourier transform (12). This property makes it straightforward to compare measurements made at different times at possibly different physical locations. The measurement system extends the capabilities of a spectrum analyser, by returning both magnitude and phase information. The phase spectrum, is dependent on relative time-shift, making it difficult to compare measurements, or incorporate several measurements made at different times into a model. The Fourier transform of a time shifted waveform is given in (12), expanded into magnitude and phase.

$$\begin{aligned} f(t + t_0) &\leftrightarrow F(\omega)e^{j\omega t_0} \\ &\leftrightarrow |F(\omega)|\angle\varphi[F(\omega)] + \omega t_0 \end{aligned} \quad (12)$$

where  $f(t + t_0)$  is a time-domain function with time shift of  $t_0$ ,  $F(\omega)$  the frequency spectrum corresponding to  $f(t)$ ,  $\omega$  the angular frequency and  $\varphi(x)$  is a function that returns the angle associated with the complex quantity  $x$

The difficulty is in finding the relative time-shift between two measurements made at different times, in the presence of measurement noise and without an absolute time-reference. Fig. 4 is an example of the phase measured over time. The phase varies slowly over time due to imperfect phase locking in the system.

In linear systems this issue is resolved by applying the principle of superposition. Each frequency component can be treated individually and superposition applied to construct the response of a complex waveform. Therefore a linear

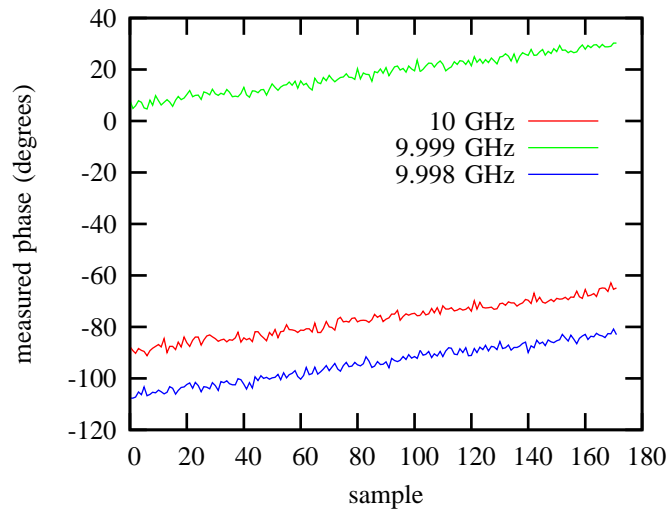


Fig. 4. Measured phase over samples for three tones in the multi-tone signal. The measured phase varies slowly over time due to the imperfect phase locking in the system.

transfer function can be reported at each frequency of interest, the transfer function being time-invariant for most devices.

There are two methods for dealing with time-variant phase in nonlinear systems, phase detrending [5] and time-invariant phase definitions [6] [7] [8] [9]. Phase detrending has the advantage of good noise immunity but requires prior knowledge of the approximate measurement phase. Time-invariant phase definitions do not require prior knowledge, but perform poorly in the presence of measurement noise.

## PHASE DETRENDING

In phase detrending the goal is to calculate the relative time-shift between two sets of measurements or a measurement and a target result (ie. a simulation result). For detrending measurements that contain noise, a least squares (or a weighted least squares) problem is formulated. The minimization problem is of the form:

$$\begin{aligned} & \min E(t) \\ & \text{subject to:} \\ & E(t) = \sum_{i=1}^N |\theta_i(t) - \theta_{i,target}|^2 \end{aligned} \quad (13)$$

where  $E(t)$  is the function to minimize,  $t$  the time shift,  $\theta_i(t)$  a vector of phases with index  $i$  and  $\theta_{i,target}$  the vector of target phases with index  $i$ .

A graphical example of the problem is shown in Fig. 5. This nonlinear problem is difficult to solve due to the large number of local minimums. One solution consists of determining an initial solution estimate, then searching the local minimums around that estimate for the global solution [5].

## TIME-INVARIANT PHASE DEFINITIONS

For many applications, such as behavioural modeling, a target phase is not known. Therefore, useful methods that do not require prior knowledge about the signal to be measured are time-invariant phase definitions [6] [7] [8] [9]. Time-invariant phase definitions are an abstraction of the measured phase, which do not depend on the time the measurement was performed.

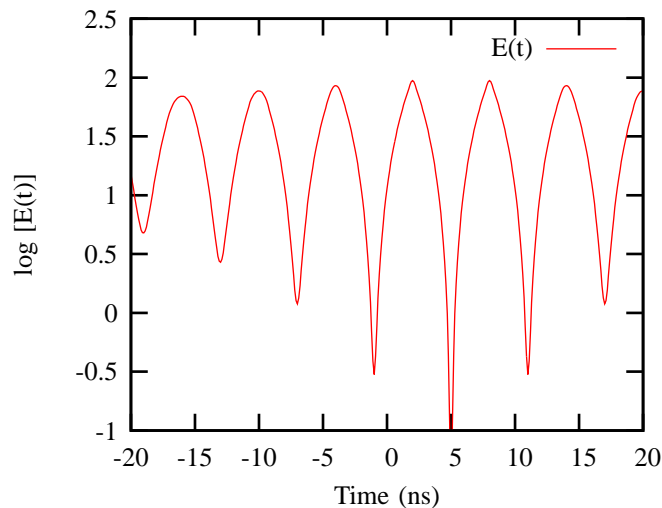


Fig. 5. Plot of the error function  $E(t)$ . The function has many local minimums which make evaluation of the global minimum difficult. This example has the solution at  $t = 5ns$

The simplest approach [6] is to consider the relationship between the harmonically related frequency components. Take the frequency components  $\omega_A$  and  $\omega_B$  with phases  $\Phi_A$  and  $\Phi_B$  respectively. The time-invariant phase of  $\omega_A$  denoted  $\Phi'_A$  is set to zero and then the time-invariant phase of the component at  $\omega_B$  denoted  $\Phi'_B$  is given by:

$$\begin{aligned}\Phi'_B &= (\Phi_B + \omega_B t_0) - \frac{\omega_B}{\omega_A}(\Phi_A + \omega_A t_0) \\ \Phi'_B &= \Phi_B - \frac{\omega_B}{\omega_A}\Phi_A\end{aligned}\quad (14)$$

where  $\omega_B = n\omega_A$ ,  $n$  an integer ( $n \geq 1$ ),  $t_0$  an arbitrary phase shift and the phases are modulo  $2\pi$  (ie.,  $0^\circ \leq \Phi \leq 2\pi$ ). For the case where the phases are not harmonically related, referencing the phase to two different frequencies for which the frequencies of interest are a combination has been proposed in [7]. Practical frequencies are the smallest modulation frequency and the carrier frequency.

Given the following definition for the frequency  $f_{k,m}$ :

$$f_{k,m} = kf_p + mf_0 \quad (15)$$

where  $k$  and  $m$  are a linear combination of the pump frequency  $f_p$  and an offset frequency  $f_0$  (in practice  $f_0$  is the greatest common divisor of the frequencies of interest).

The time-invariant phase can then be redefined as

$$\Phi'_{k,m} = \Phi_{k,m} - (k\Phi_p + m\Phi_0) \quad (16)$$

where  $\Phi'_{k,m}$  is the time-invariant phase and  $\Phi_{k,m}$  the time-variant phase at  $f_{k,m}$ ,  $\Phi_p$  the time-variant phase at the pump frequency and  $\Phi_0$  the time-variant phase at the offset frequency.

Typically a multi-tone signal has no energy at the smallest modulation frequency, therefore the phase of ( $f_0$ ) is chosen to be the difference in phase between two adjacent tones. The new equation becomes:

$$\begin{aligned}\Phi'_{k,m} &= \Phi_{k,m} - (k\Phi_p + m\Phi_0) \\ &= \Phi_{k,m} - (k+m)\Phi_p + m\Phi_q\end{aligned}\quad (17)$$

where  $\Phi_0 = \Phi_p - \Phi_q$  and  $\Phi_q$  is the phase of a frequency adjacent to  $f_p$ .

These methods are generally simple to compute and do not require prior knowledge about the signal to be measured, however appear to have poor immunity to measurement noise.

## MEASUREMENT COMPARISON

While both the phase detrending and time-invariant phase definitions perform equally well when the phase is perfectly known, the transforms are affected differently by measurement noise. Phase detrending appears to have lower variance after the transform is applied. This proposition was confirmed by measuring a multi-tone signal and applying both the detrending and time-invariant phase transforms.

A multi-tone signal consisting of 41 pseudo-random phase tones spaced 1 MHz apart centered around 10 GHz (10 GHz carrier with 20 tones spaced either side) was generated with an Agilent E8267C PSG. The source, local oscillator and receivers were phase locked via the 10MHz reference and hence the phase varies slowly with time as can be seen in Fig. 4.

The sample variance was calculated from 172 measurements. To calculate the variance in the time-variant phase, a linear regression was performed and the sample variance calculated from the residuals. The detrending method was implemented using MATLAB<sup>1</sup> code from [5], which solves (13). For this measurement, the phase of the first measurement is used as the prior knowledge required to detrend the remaining 171 measurements. The time-invariant phase was computed using (17).

<sup>1</sup>MATLAB is a registered trademark of The MathWorks, Inc.

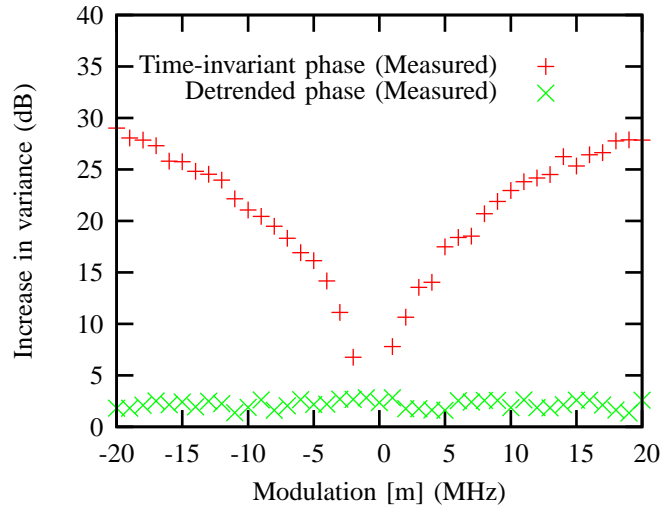


Fig. 6. Comparison of the increase in variance in a multi-tone measurement, for the phase detrending and time-invariant phase methods. While the time-invariant phase does not require prior knowledge about the signals to be measured, it has higher measurement uncertainty than the raw time-variant phase and the phase detrending method.

The increase in the variance for the detrended phase and time-invariant phase from the variance in the raw phase is shown in Fig. 6. It can be seen that the detrending method performs significantly better in the presence of measurement noise than the time-invariant phase method.

While the detrending method performs better in the presence of measurement noise, the method requires prior knowledge of the explicit phase relationship between the measured components. This may not be known in many measurement scenarios.

## APPLICATIONS

The measurement system has two key strengths, wide-bandwidth high dynamic range measurement and fully calibrated, traceable measurements. This measurement ability allows for improved measurement of wide-bandwidth signals and system, simplified extraction of circuit models, simplified extraction of coefficients for linearizers and extraction of newer behavioural models.

Nonlinear circuit and behavioural models are commonly used to model active devices. Circuit models are based on the physical devices, while behavioural models simply mimic the behaviour of the device that was simulated or measured.

Nonlinear models of active devices are often derived from measurements of real devices. Typically this is achieved by making linear S-parameter measurements and dc IV (current voltage) measurements of a test device. It has been found that these measurements are not able to fully characterize active devices such as a Gallium Arsenide (GaAs) and the newer Gallium Nitride (GaN) transistors.

The nonlinear transfer function of typical microwave transistors is different at microwave frequencies (greater than 1 GHz), than at dc where the devices are often measured. This has led to the development of techniques, such as pulsed IV, able to overcome some of the limitations of dc measurements. Pulsed IV systems are able to measure the nonlinear transfer characteristic at higher frequencies, tens of MHz, rather than at dc. These systems lack dynamic range and the transistor characteristic in some devices has been found to change up to the low gigahertz [10].

The new measurement system is able to measure transistor characteristics at microwave frequencies (up to 20 GHz) with high dynamic range. This allows the characterization of devices with excitations similar to those used in the intended application. Circuit-based models or more abstract behavioural models can therefore be extracted at high frequency with high dynamic range.

## CIRCUIT MODELS

In a circuit model, the physical structure of the device is modeled with lumped elements. Due to the underlying physics, these models scale well with changes in device dimension and can extrapolate outside the measurement data region.

Circuit models have linear lumped elements and nonlinear lumped elements as can be seen in Fig. 7. In general the linear and nonlinear elements are extracted separately. Linear lumped elements, such as model extrinsics can be extracted with a linear vector network analyser. Traditionally, the nonlinear elements are extracted with dc IV, multi-bias S-parameters, pulsed IV or spectrum analyser measurement [11]. The spectrum analyser method has the advantage of high dynamic range, but lacks phase information of the harmonics, which can be important for extracting the nonlinear drain conductance [12]. The gate charge nonlinearity extraction using a spectrum analyser [13], can be greatly simplified and dynamic range increased with the inclusion of phase information.

The new system not only extends the capabilities of a spectrum analyser by providing wide-bandwidth phase information, but is fully calibrated like a linear vector network analyser, and can thus be used to extract all the linear circuit model elements. This simplifies model extraction, as the one instrument is capable of fulfilling all the measurement requirements for extracting the model.

## BEHAVIOURAL MODELS

Behavioural models mimic the behaviour of the device that was measured. They are based on purely mathematical functions and as such little information about the device physics can be inferred from these models. This can be useful for protecting trade secrets, while allowing models to be widely distributed in computer aided design (CAD) packages. These models are also useful for new fabrication processes, where good physical models have yet to be developed. Behavioural models also tend to be simpler, often leading to reduced simulation times. These models typically do not extrapolate well outside the measurement data region.

Nonlinear network analysers are an ideal instrument type for extracting behavioural models. A behavioural model assumes nothing about the device being measured, so complete information about the incident and reflected waves at both ports is required to make the extraction. Often the models are extracted with the actual signals the device is intended to be operated with. For instance a W-CDMA signal might be used where the models is used in the design of systems for mobile phone applications.

Behavioural models can be constructed in the time-domain [14] (nonlinear time-series analysis) or in the frequency domain such as the Poly-Harmonic Distortion (PHD) model [15]. Nonlinear time-series models are generally based on polynomial or artificial neural networks. Polynomial models are simple to fit (a linear optimization algorithm can be used), while artificial neural networks saturate, providing more realistic behaviour outside the measurement region.

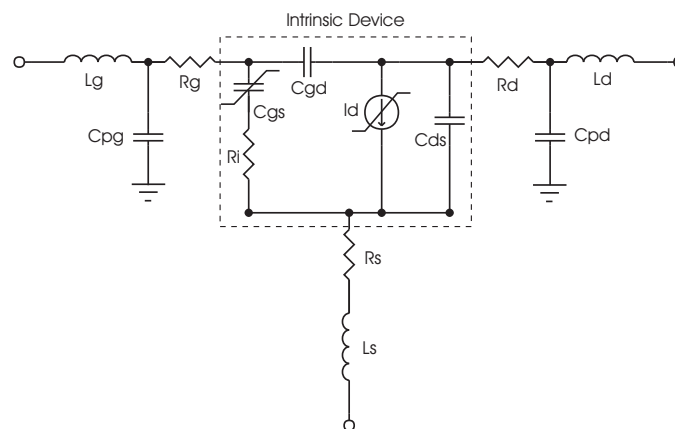


Fig. 7. Example of a nonlinear circuit model. The model contains both linear and nonlinear lumped elements. The intrinsic elements represent the active portion of the transistor.

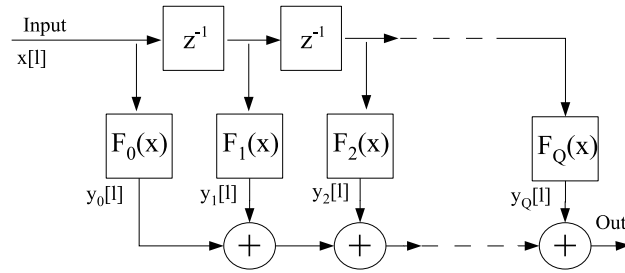


Fig. 8. Example of a nonlinear time series model based on polynomials [16].  $F_Q(x)$  is a polynomial function and  $z^{-1}$  a time delay.

An example of a behavioural model based on polynomials is given in [16] and reproduced in Fig. 8.

## CONCLUSION

A measurement system that offers superior performance has been presented. The system can accurately measure devices at a connectorized plane or on-wafer, allowing the extraction of circuit models, behavioural models and linearizer coefficients. This leads to improved circuit design and simplified development process.

## References

- [1] P. S. Blockley, D. Gunyan, and J. B. Scott, "Mixer-based, vector-corrected, vector signal/network analyzer offering 300kHz-20GHz," in *IEEE International Microwave Symposium Digest*, June 2005.
- [2] D. Rytting, "Network analyzer error models and calibration methods." White Paper, September 1998, Hewlett-Packard Company.
- [3] J. B. Scott, P. S. Blockley, and A. E. Parker, "A new instrument architecture for millimetre-wave time-domain signal analysis," in *63th ARFTG Conference Digest*, pp. 47–52, June 2004.
- [4] J. Verspecht, P. Debie, A. Barel, and L. Martens, "Accurate on wafer measurement of phase and amplitude of the spectral components of incident and scattered voltage waves at the signal ports of a nonlinear microwave device," in *IEEE International Microwave Symposium Digest*, pp. 1029–1032, May 1995.
- [5] K. A. Remley, D. F. Williams, D. M. M.-P. Schreurs, G. Loglio, and A. Cidronali, "Phase detrending for measured multisine signals," in *61th ARFTG Conference Digest*, June 2003.
- [6] J. Jargon, D. DeGroot, K. C. Gupta, and A. Cidronali, "Calculating ratios of harmonically related, complex signals with application to nonlinear large-signal scattering parameters," in *60th ARFTG Conference Digest*, 2002.
- [7] G. Loglio, J. Jargon, and D. C. DeGroot, "Phasor angle definition suitable for intermodulation measurements," in *65th ARFTG Conference Digest*, June 2005.
- [8] J. C. Pedro, J. P. Martins, and P. M. Cabral, "New method for phase characterization of nonlinear distortion products," in *IEEE International Microwave Symposium Digest*, June 2005.
- [9] T. Nakatani, T. Matsuura, and K. Ogawa, "A simple method for measuring the IM3 components of multi-stage cascaded power amplifiers considering the phase characteristics," in *IEEE International Microwave Symposium Digest*, June 2004.
- [10] A. E. Parker and J. G. Rathmell, "Novel technique for determining bias, temperature and frequency dependence of FET characteristics," in *IEEE International Microwave Symposium Digest*, pp. 993–996, June 2002.
- [11] J. C. Pedro and J. Perez, "Accurate simulation of GaAs MESFET's intermodulation distortion using a new drain-source current model," *IEEE Transactions on Microwave Theory and Techniques*, pp. 25–33, Jan. 1994.
- [12] J. Brinkhoff and A. E. Parker, "Charge trapping and intermodulation in HEMTs," in *IEEE International Microwave Symposium Digest*, pp. 799–802, June 2004.
- [13] J. A. Garcia, A. M. Sanchez, J. Pedro, N. B. D. Carvalho, A. T. Puente, and J. L. Garcia, "Characterizing the gate-to-source nonlinear capacitor role on GaAs FET imd performance," *IEEE Transactions on Microwave Theory and Techniques*, pp. 2344–2355, Dec. 1998.
- [14] D. Schreurs, J. Wood, N. Tufillaro, D. Usikov, L. Barford, and D. E. Root, "The construction and evaluation of behavioral models for microwave devices based on time-domain large-signal measurements," in *IEDM Technical Digest. International Electron Devices Meeting*, pp. 819–822, 2000.
- [15] J. Verspecht, D. E. Root, J. Wood, and A. Cognata, "Broad-band, multi-harmonic frequency domain behavioral models from automated large-signal vectorial network measurements," in *IEEE International Microwave Symposium Digest*, June 2005.
- [16] H. Qian, L. Ding, G. T. Zhou, and J. S. Kenney, "Predistortion linearization results for power amplifiers with memory effects," in *IEEE Topical Workshop on Power Amplifiers*, Sept. 2004.